Journal of Luminescence 177 (2016) 254–260

Contents lists available at ScienceDirect

Journal of Luminescence

journal homepage: www.elsevier.com/locate/jlumin

Full Length Article

# The d–f luminescence of $Eu^{2+}$, $Ce^{3+}$ and $Yb^{2+}$ ions in $Cs_2MP_2O_7$ ($M = Ca^{2+}$, $Sr^{2+}$)

Tim Senden [a,*], Andries Meijerink [a]

[a] Condensed Matter and Interfaces, Debye Institute for Nanomaterials Science, Utrecht University, P.O. Box 80 000, 3508 TA Utrecht, The Netherlands

ARTICLE INFO

*Article history:*
Received 22 February 2016
Accepted 29 April 2016
Available online 5 May 2016

*Keywords:*
$Cs_2MP_2O_7$ ($M = Ca^{2+}$, $Sr^{2+}$)
Lanthanide d–f luminescence
Stokes shift
Jahn-Teller deformation

ABSTRACT

The efficient narrow band emission of $Eu^{2+}$ in $Cs_2MP_2O_7$ ($M = Ca^{2+}$, $Sr^{2+}$) is characterized by a large Stokes shift and a high quenching temperature which makes the material promising for application in warm white LEDs. The unusual $Eu^{2+}$ luminescence properties were reported recently but an explanation for the peculiar behavior is lacking. In this paper we aim at providing new insights in the luminescence of the $Eu^{2+}$ emission in $Cs_2MP_2O_7$ through measurements at cryogenic temperatures (down to 4 K) and by comparison with the d–f luminescence of $Ce^{3+}$ and $Yb^{2+}$ in the same host. The results reveal a sharp onset of the $Eu^{2+}$ emission and excitation bands at 4 K. Usually the sharp onset for narrow excitation and emission bands coincide at an energy corresponding to the zero-phonon (purely electronic) transition, but for $Eu^{2+}$ in $Cs_2MP_2O_7$ there is a large shift of 3500 $cm^{-1}$ between the onsets, consistent with the large Stokes shift observed. The onset shift can be explained by emission from a lower energy distorted excited $4f^65d^1$ state. For $Ce^{3+}$, the f–d absorption bands are at energies expected based on the relation between the absorption energies for $Eu^{2+}$ and $Ce^{3+}$ reported by Dorenbos. Contrary to $Eu^{2+}$, the emission for $Ce^{3+}$ shows a normal Stokes shift and therefore the emission bands are at much higher energies than predicted from the energy of the $Eu^{2+}$ emission and the Dorenbos relations. Based on the present results the unusually large Stokes shift for the $Eu^{2+}$ emission in $Cs_2MP_2O_7$ is assigned to a Jahn–Teller like deformation in the excited $4f^65d^1$ state of $Eu^{2+}$ that is not present in the 5d state of $Ce^{3+}$.



## 1. Introduction

The optical properties of the $Eu^{2+}$ ion ($4f^7$) have been thoroughly investigated [1–5] and the efficient luminescence of $Eu^{2+}$ is widely applied, e.g. in fluorescent tubes, white light LEDs (wLEDs), displays, scintillators and anti-counterfeiting labels [6–10]. The emission and absorption spectra of $Eu^{2+}$ are characterized by broad absorption and emission bands corresponding to transitions between the $4f^7$ ground state and the $4f^65d^1$ excited states. The energy level structure in the $4f^65d^1$ excited state is strongly influenced by covalency and crystal field splitting [8]. As a result, the d–f emission of $Eu^{2+}$ can vary from the ultraviolet to the red spectral region, depending on the host lattice.

In phosphates $Eu^{2+}$ ions typically show a violet or blue emission and emission wavelengths between 375 nm (for $Ba(PO_3)_2$:$Eu^{2+}$) and 505 nm (for $NaCaPO_4$:$Eu^{2+}$) have been reported [1]. However, recently an unusual red $Eu^{2+}$ emission was reported for a $Eu^{2+}$-doped phosphate. In $Cs_2CaP_2O_7$ the d–f emission of $Eu^{2+}$ is around 600 nm, while the absorption is in the usual blue-ultraviolet spectral region [11]. As a result, the Stokes shift of the emission is very large ($\Delta S > 6000\ cm^{-1}$). The emission is further characterized by a high quantum yield and a high quenching temperature ($T_{0.5} \sim 600$ K), which is unexpected in combination with a large Stokes shift [8]. The special optical properties make $Cs_2CaP_2O_7$:$Eu^{2+}$ promising as a red emitting phosphor in warm white LEDs, where a narrow band red emission is required to reduce efficiency loss that is inherent to the use of broad band red emitters. Broad band red emitters that are used to shift the color temperature of wLEDs into the desired warm white spectral region have a significant part of their emission between 630 and 700 nm where the eye sensitivity is low. This reduces the lumen/W efficiency [9].

The large Stokes shift and narrow band emission reported for $Eu^{2+}$ in $Cs_2MP_2O_7$ ($M = Ca^{2+}$, $Sr^{2+}$) were discussed by Srivastava et al. [11]. Based on the narrow band emission ($I^{em} \sim 2000\ cm^{-1}$ at 80 K), normal emission lifetime ($\tau \sim 1$ μs) and high quenching temperature ($T_{0.5} \sim 600$ K) it was concluded that the large Stokes shift cannot be explained by anomalous emission from an Eu-trapped exciton state. In the past large Stokes shifts for $Eu^{2+}$ emission have been explained by a trapped exciton emission, but in addition to a large Stokes shift, this emission is characterized by a large spectral width, longer lifetime and low quenching

* Corresponding author.
*E-mail address:* t.senden@uu.nl (T. Senden).

http://dx.doi.org/10.1016/j.jlumin.2016.04.050
0022-2313/

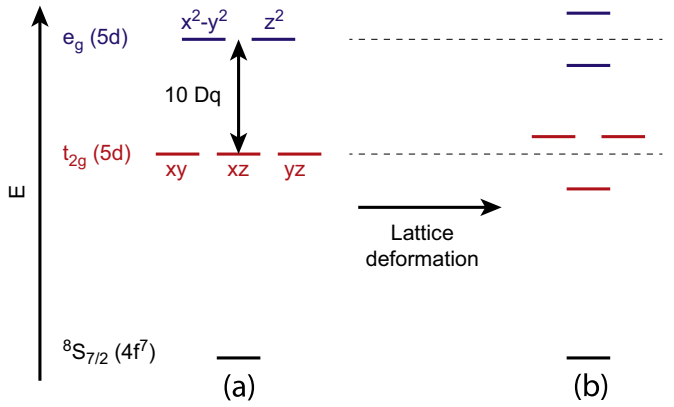


**Fig. 1.** Schematic representation of the $Eu^{2+}$ energy level scheme in (a) octahedral and (b) strongly deformed configuration.

temperature [2]. Clearly, these characteristics are not observed for the $Eu^{2+}$ emission in $Cs_2MP_2O_7$. An alternative explanation that was suggested in Refs. [11,12] involves distortions in the $4f^65d^1$ excited state. In $Cs_2MP_2O_7$ the $Eu^{2+}$ ion is in an octahedral coordination. In Fig. 1 the crystal field splitting in $O_h$ symmetry is illustrated. In the excited 5d state a, for example, tetragonal deformation can lower the energy of the lowest $4f^65d^1$ state as illustrated in Fig. 1. Emission from the lowest $4f^65d^1$ state will be shifted to a lower energy and can explain the large Stokes shift.

Substantial lattice deformations in the 5d excited state have previously been shown to give rise to large Stokes shifts ($\Delta S > 5000\ cm^{-1}$) for d–f emission of $Ce^{3+}$ in halides [13–16]. As an example, for $LaCl_3:Ce^{3+}$ ($\Delta S = 5800\ cm^{-1}$) it was found with ab initio calculations that in the excited $5d^1$ configuration there is an off-center movement of the $Ce^{3+}$ ion, which is accompanied by a strong deformation of the ligand prism around the $Ce^{3+}$ ion [14]. Due to this deformation the crystal field splitting almost doubles, resulting in a very large Stokes shift. The results also explained why the concentrated system $CeCl_3$, despite having the same crystal structure as $LaCl_3$, had a very small Stokes shift of only $900\ cm^{-1}$. It was found that in $CeCl_3$ the more stable off-center $Ce^{3+}$ position is already occupied in the ground state $4f^1$ configuration, resulting in a small Stokes shift. It was determined that the off-center movement of the $Ce^{3+}$ ion is due to a reorientation of the occupied 5d orbital by a (pseudo) Jahn–Teller mixing between the two lowest 5d states, as these are very close in energy [16]. A similar Jahn–Teller type deformation may play a role in explaining the large Stokes shift for $Cs_2MP_2O_7:Eu^{2+}$.

To investigate the origin of the large Stokes shift for the $Eu^{2+}$ emission in $Cs_2MP_2O_7$ here we report luminescence spectra recorded at cryogenic temperatures. At low temperatures often zero-phonon lines and sharp onsets of excitation and emission spectra are observed which give information on the energy of the electronic origin of excited states involved. A shift of the zero-phonon line or sharp onset between emission and excitation spectra can provide evidence for electronic relaxation in the excited state. In addition, the d–f luminescence for other lanthanide ions, $Ce^{3+}$ and $Yb^{2+}$, is investigated and compared with the luminescence properties of $Eu^{2+}$. The results reveal a large shift between the sharp onset in the excitation and emission spectra of $Eu^{2+}$. Contrary to the unusually large Stokes shift and red-shifted emission observed for $Eu^{2+}$ in $Cs_2MP_2O_7$, the luminescence of $Ce^{3+}$ is normal in $Cs_2MP_2O_7$ indicating that the unusual luminescence properties are specific for the d–f emission of $Eu^{2+}$.

## 2. Experimental

Microcrystalline samples of $Cs_2MP_2O_7$ ($M = Ca^{2+}, Sr^{2+}$) doped with 0.1 or 1% of $Eu^{2+}$, $Ce^{3+}$ or $Yb^{2+}$ ions were synthesized using solid-state reaction techniques. The starting materials $Cs_2CO_3$ (10 mole% excess), $(NH_4)_2HPO_4$ (10 mole% excess), CaO, $SrCO_3$ and $Eu_2O_3$, $Yb_2O_3$ or $CeO_2$ were thoroughly mixed and ground with a pestle in an agate mortar. The powder mixtures were dried at 300 °C for 1 h in air and, subsequently, fired twice at 750 °C ($Cs_2CaP_2O_7$) or 800 °C ($Cs_2SrP_2O_7$) for 5 h in a reducing atmosphere (10% $H_2$/90% $N_2$). The samples were thoroughly ground between each heating step. X-ray diffraction measurements confirmed that the $Cs_2CaP_2O_7$ and $Cs_2SrP_2O_7$ powders were single phase (see Fig. S1).

Photoluminescence (PL) spectra and decay curves of the samples were measured using an Edinburgh Instruments FLS920 fluorescence spectrometer, equipped with a 450 W xenon lamp as excitation source, a double excitation monochromator (0.22 m) and a single emission monochromator (0.22 m). For measurements down to 4 K, the samples were cooled in an Oxford Instruments liquid helium flow cryostat. Emission was detected with a Hamamatsu R928 photomultiplier tube (PMT). For lifetime measurements, $Ce^{3+}$ ions were excited with a PicoQuant pulsed diode (PDL 800-B combined with PLS 270, $\lambda_{exc} = 270$ nm, pulse width 650 ps) and $Eu^{2+}$ was excited with an Edinburgh EPL375 pulsed diode laser ($\lambda_{exc} = 376.8$ nm, pulse width 65 ps). The decay curves were recorded with a Hamamatsu H74422–40 PMT.

Excitation spectra in the deep UV and vacuum ultraviolet (VUV) region (between 150 and 300 nm) were recorded at the BL3B beamline of the UVSOR facility (Okazaki, Japan). This beamline consists of a 2.5 m off-plane Eagle type normal incidence monochromator, which covers the VUV, UV and visible (VIS) regions. In the present experiments a spherical grating with a groove density of 600 lines/mm optimized at a photon energy of ~16 eV was used. For the photoluminescence measurements in the UV-VIS region, a 0.22 m Acton monochromator with a Princeton Instruments CCD detector was used. Excitation spectra were recorded using a Hamamatsu R4220 PMT connected to the same monochromator.

## 3. Results and discussion

### 3.1. $Eu^{2+}$ luminescence

To investigate the origin of the large Stokes shift luminescence spectra were recorded at cryogenic temperatures. At 4 K only the lowest vibrational level in the ground and excited states are thermally populated resulting in narrow bands in emission and excitation. Also, in case of weak electron-phonon coupling (small Huang–Rhys parameter $S$) zero-phonon lines may be observed in excitation and emission. For a specific electronic transition the zero-phonon line in excitation and emission are expected at the same energy, as has been observed for e.g. $Eu^{2+}$ and $Ce^{3+}$ [17–20]. Figs. 2 and 3 show the emission (red lines) and excitation spectra (blue lines) at $T = 4$ K of $Cs_2CaP_2O_7:Eu^{2+}$ (1%) and $Cs_2SrP_2O_7:Eu^{2+}$ (0.1%), respectively. The blue solid lines are the excitation spectra that were measured using the Edinburgh Instruments FLS920 fluorescence spectrometer and the blue broken lines are the excitation spectra that were recorded at beamline BL3B of the UVSOR facility.

In the excitation spectra a broad band is observed between 22 500 and 35 000 $cm^{-1}$, which is assigned to the $Eu^{2+}$ $4f^7 \rightarrow 4f^65d^1(t_{2g})$ transition. At higher energy, around 45 000 $cm^{-1}$, another absorption band is observed that is assigned to the $Eu^{2+}$ $4f^7 \rightarrow 4f^65d^1(e_g)$ transition. The lower energy band shows the characteristic staircase

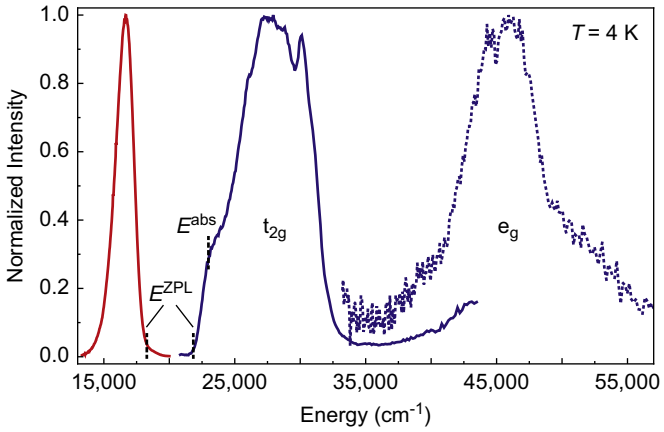


**Fig. 2.** The emission (red line; $\lambda_{exc} = 340$ nm) and (V)UV excitation spectra (blue solid line; $\lambda_{em} = 630$ nm and blue dashed line; $\lambda_{em} = 640$ nm) of $Cs_2CaP_2O_7$:$Eu^{2+}$ (1%) at $T = 4$ K. The spectra recorded with the Edinburgh Instruments FLS 920 fluorescence spectrometer are the solid lines and the excitation spectrum measured at the UVSOR facility is the dotted line. (For interpretation of the references to color in this figure caption, the reader is referred to the web version of this paper.)

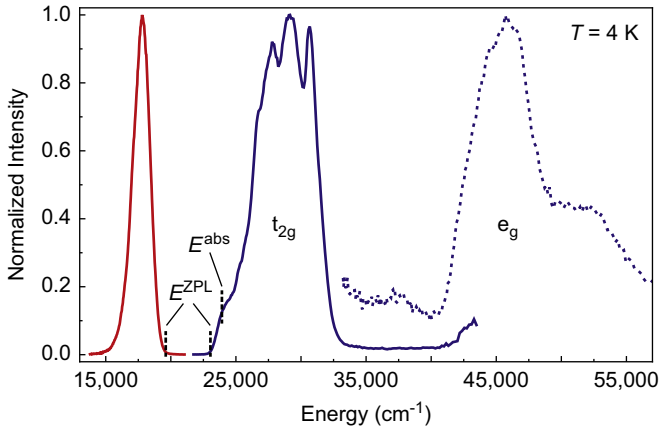


**Fig. 3.** The emission (red line; $\lambda_{exc} = 340$ nm) and (V)UV excitation spectra (blue solid line; $\lambda_{em} = 570$ nm and blue dashed line; $\lambda_{em} = 560$ nm) of $Cs_2SrP_2O_7$:$Eu^{2+}$ (0.1%) at $T = 4$ K. The spectra recorded with the Edinburgh Instruments FLS 920 fluorescence spectrometer are the solid lines and the excitation spectrum measured at the UVSOR facility is the dotted line. (For interpretation of the references to color in this figure caption, the reader is referred to the web version of this paper.)

structure of a $Eu^{2+}$ $4f^7 \rightarrow 4f^6\left[^7F_J\right]5d^1$ absorption band, which is caused by transitions to the seven $^7F_J$ ($J = 0-6$) multiplets of the $4f^6$ configuration in the $4f^65d^1$ excited state.

In order to calculate the crystal field splitting 10 Dq, we determine the energy difference between the onsets of the $t_{2g}$ and $e_g$ absorption bands. We find a crystal field splitting of 18 982 $cm^{-1}$ for $Cs_2CaP_2O_7$ and 17 281 $cm^{-1}$ for $Cs_2SrP_2O_7$. Alternatively, we can estimate the crystal field splitting by taking the energy difference between the maximums of $t_{2g}$ and $e_g$ absorption bands. Using this method, a crystal field splitting of 17 677 $cm^{-1}$ and 16 422 $cm^{-1}$ for $Cs_2CaP_2O_7$ and $Cs_2SrP_2O_7$, respectively. The results show that the crystal field splitting is larger in $Cs_2CaP_2O_7$ than in $Cs_2SrP_2O_7$, in agreement with Ref. [11]. The stronger crystal field splitting for $Eu^{2+}$ in $Cs_2CaP_2O_7$ is consistent with the shorter $Eu^{2+}-O^{2-}$ distance in $Cs_2CaP_2O_7$.

The emission spectrum of $Eu^{2+}$ activated $Cs_2CaP_2O_7$ and $Cs_2SrP_2O_7$ at $T = 4$ K is a narrow asymmetrical band centered around a peak energy $E^{em}$ of 16 694 $cm^{-1}$ (599 nm) and 17 857 $cm^{-1}$ (560 nm) with a full width at half maximum intensity $I^{em}$ of 1618 and 1506 $cm^{-1}$, respectively (see Figs. 2 and 3 and Table 1). At room temperature the emission bands are more symmetrical and broader (see Fig. S2), with a $I^{em}$ that has increased to 3045 $cm^{-1}$ for M = $Ca^{2+}$ and to 3138 $cm^{-1}$ for M = $Sr^{2+}$. The increase in emission bandwidth is due to thermal broadening. Previously it was reported that $I^{em}$ is 2191 and 2147 $cm^{-1}$ at $T = 80$ K for M = $Ca^{2+}$ and $Sr^{2+}$, respectively [11]. These values fit nicely between the $I^{em}$ values we have obtained at $T = 4$ K and room temperature. Besides an increase in bandwidth, the $E^{em}$ has slightly shifted to higher energy (a blue shift of approximately 10 nm) when the temperature is increased to 298 K (see Fig. S2). The shift in $E^{em}$ is attributed to emission from thermally occupied higher vibrational levels in the excited state and/or a small decrease in the crystal field strength when the temperature increases (longer $Eu^{2+}-O^{2-}$ distance). The luminescence properties in Figs. 2 and 3 are in agreement with the results previously reported for $Cs_2MP_2O_7$:$Eu^{2+}$ at 80 K in Ref. [11]. However, the spectra shown in this work were recorded at 4 K instead of 80 K. At 4 K (the onsets of) the emission and excitation bands are better resolved, which is important for e.g. correctly determining the Stokes shift of the $Eu^{2+}$ emission.

**Table 1**
Optical properties of $Eu^{2+}$ ions in $Cs_2CaP_2O_7$ and $Cs_2SrP_2O_7$. Peak energy of the emission band $E^{em}$, full width at half maximum intensity of the emission band $I^{em}$, estimated energy of the $4f^7 \rightarrow 4f^6\left[^7F_0\right]5d^1$ transition $E^{abs}$ and the Stokes shift $\Delta S = E^{abs} - E^{em}$. All values are in $cm^{-1}$ and at $T = 4$ K.

| Host | $E^{em}$ | $I^{em}$ | $E^{abs}$ | $\Delta S$ |
|---|---|---|---|---|
| $Cs_2CaP_2O_7$ | 16 694 | 1618 | 22 989 | 6294 |
| $Cs_2SrP_2O_7$ | 17 857 | 1506 | 23 923 | 6066 |

The $Eu^{2+}$ emission is in the red ($Cs_2CaP_2O_7$:$Eu^{2+}$) or yellow ($Cs_2SrP_2O_7$:$Eu^{2+}$) spectral region, which is highly unusual for $Eu^{2+}$ in a phosphate host lattice. The low energy luminescence originates from the very large $Eu^{2+}$ Stokes shift ($\Delta S$). $\Delta S$ of the $Eu^{2+}$ emission is defined as the difference between the energy of the $4f^7 \rightarrow 4f^6\left[^7F_0\right]5d^1$ transition $E^{abs}$ and the peak energy of the emission band $E^{em}$. The transition from the $4f^7$ $^8S_{7/2}$ ground state to the $4f^6\left[^7F_0\right]5d^1$ excited state corresponds to the first "step" in the characteristic staircase structure of the f–d absorption band. However, if the first step is not resolved in the spectra, $E^{abs}$ can be determined by taking the energy at which, on the low-energy side, the excitation band has risen to 15–20% of the maximum of the "staircase" [1].

The values for $E^{abs}$ and $E^{em}$ are most accurately determined at cryogenic temperatures, as at 4 K there is least thermal broadening of the emission and excitation bands. Hence, the first step in the staircase is clearly resolved in our excitation spectra measured at 4 K (see Figs. 2 and 3). By locating the first step in the staircase structure, it is estimated that $E^{abs} = 22\,989$ $cm^{-1}$ for $Cs_2CaP_2O_7$ and 23 923 $cm^{-1}$ for $Cs_2SrP_2O_7$ (see also Table 1). The $E^{abs}$ is lower for $Cs_2CaP_2O_7$ compared to $Cs_2SrP_2O_7$ as the stronger crystal field splitting in $Cs_2CaP_2O_7$ shifts the lowest $4f^65d^1$ state to lower energies.

The values we find for $E^{abs}$ are approximately 2000 $cm^{-1}$ lower in energy compared to those reported in Ref. [11]. However, in Ref. [11] a different method was used to estimate $E^{abs}$. Instead of using the common method to locate $E^{abs}$ at the first step in the staircase, $E^{abs}$ was determined by first fixing the $^7F_6$ level on the highest energy peak in the excitation spectra and then use a 5080 $cm^{-1}$ multiplet splitting of the $Eu^{3+}$ $^7F_J$ term to locate the position of the $4f^6\left[^7F_0\right]5d^1$ level. However, the splitting of the $^7F_J$ multiplets in the $4f^65d^1$ state is often larger than the $\sim 5080$ $cm^{-1}$ observed for $Eu^{3+}$ [1,21], explaining the difference in $E^{abs}$ between Ref. [11] and the present work.

Using the values determined for $E^{abs}$ and $E^{em}$, we calculate the Stokes shift $\Delta S = E^{abs} - E^{em}$. It is found that $\Delta S = 6294$ and 6066 $cm^{-1}$ for M = $Ca^{2+}$ and $Sr^{2+}$, respectively (see Table 1). The estimated $\Delta S$ are approximately 2000 $cm^{-1}$ smaller compared to what is reported in Ref. [11], consistent with the lower values determined for $E^{abs}$. The $\Delta S$ values are significantly larger than the typical Stokes shift of $\Delta S = 1000–2000$ $cm^{-1}$ observed for $Eu^{2+}$ d–f luminescence [1]. Moreover, the Stokes shift of $Eu^{2+}$ in $Cs_2MP_2O_7$ is larger than the largest Stokes shift value ever reported for $Eu^{2+}$ d–f luminescence ($\Delta S \approx 5300$ $cm^{-1}$ for $Eu^{2+}$ in $Sr_2SiO_4$) [22].

At cryogenic temperatures the Stokes shift and emission bandwidth are expected to be of similar energy [21,19]. However, this is not the case for $Eu^{2+}$ in $Cs_2MP_2O_7$ (see Table 1). In a first approximation $\Delta S$ (Eq. (1)) and $\Gamma^{em}$ (Eq. (2)) can both be interpreted in terms of the Huang–Rhys parameter $S$ and the lattice phonon energies. In the configurational coordinate model, assuming harmonic oscillators [23,24]:

$$\Delta S = (2S-1)\hbar\omega \quad (1)$$

$$\Gamma(T) \cong 2.36\hbar\omega\sqrt{S}\sqrt{\coth\frac{\hbar\omega}{2kT}} \quad (2)$$

Using Eqs. (1) and (2), we can estimate the expected Stokes shift from the emission bandwidth at 4 K, assuming that $\hbar\omega = 400$ $cm^{-1}$ for a $Eu^{2+}-O^{2-}$ vibration [24]. It is calculated that $\Delta S$ should be around 1950 and 1650 $cm^{-1}$ for $Cs_2CaP_2O_7$ and $Cs_2SrP_2O_7$, respectively. These values are significantly smaller than what is observed for $Eu^{2+}$ in $Cs_2MP_2O_7$ (see also Table 1).

The low temperature spectra shown in Figs. 2 and 3 provide information on the origin of the unusually large Stokes shift that is observed for $Eu^{2+}$ in $Cs_2MP_2O_7$. At cryogenic temperatures often zero-phonon lines and/or sharp onsets of the excitation and emission spectra are observed, coinciding on the energy of the electronic origin of excited states involved. Consequently, the low temperature spectra can show whether the emission and excitation bands used for determining the Stokes shift belong to the same electronic transition [24].

The spectra in Figs. 2 and 3 do not show any zero-phonon lines, but do reveal sharp onsets for the emission and excitation bands. Using the sharp onsets, we can estimate the energy of the zero-phonon (purely electronic) transition ($E^{ZPL}$) for the emission and excitation bands. For a specific electronic transition the sharp onsets of narrow excitation and emission bands coincide at an energy corresponding to the zero-phonon transition [17–20]. However, this is not the case for $Eu^{2+}$ in $Cs_2MP_2O_7$, as there is a large energy difference between the sharp onsets (and estimated $E^{ZPL}$) of the emission and excitation bands. It is estimated that the shift between the onsets of the $Eu^{2+}$ emission and excitation bands is around 3500 $cm^{-1}$, both for $Cs_2CaP_2O_7$ and $Cs_2SrP_2O_7$. This large "onset shift" is consistent with the large Stokes shift observed.

The large shift between the onsets of the $Eu^{2+}$ emission and excitation bands shows that different excited states are involved in the emission and absorption process. This indicates that there is a substantial electronic relaxation in the $4f^6 5d^1$ excited state, which can be due to a Jahn–Teller like deformation. As a consequence of this deformation in the excited state, the emission occurs from a lower energy excited $4f^6 5d^1$ state, resulting in a very large Stokes shift. Jahn–Teller distortions in the $Eu^{2+}$ $4f^6 5d^1$ state have e.g. previously been observed for $Eu^{2+}$ in $CaF_2$ and $SrF_2$ [25,26]. The Jahn–Teller splittings reported in Refs. [25,26] are smaller than 1000 $cm^{-1}$ and cannot explain the large Stokes shift observed for $Eu^{2+}$ in $Cs_2MP_2O_7$. However, for $Ce^{3+}$ there are several reports that substantial Jahn–Teller like deformations in the 5d excited state give rise to unusually large Stokes shifts [13–16]. For example, it was found that the large Stokes shift of $Ce^{3+}$ in $LaCl_3$ ($\Delta S = 5800$ $cm^{-1}$) is due to an off-center movement of the $Ce^{3+}$ ion accompanied by a strong deformation of the ligand prism. It was determined in Ref. [16] that the off-center movement of the $Ce^{3+}$ ion is due to a reorientation of the occupied 5d orbital by a (pseudo) Jahn–Teller mixing between the two lowest 5d states. Similar Jahn–Teller deformations can occur in the $4f^6 5d^1$ excited state of $Eu^{2+}$ in $Cs_2MP_2O_7$. Therefore, based on the results presented in this Section we assign the unusually large Stokes shift for the $Eu^{2+}$ emission in $Cs_2MP_2O_7$ to a Jahn–Teller like deformation in the excited $4f^6 5d^1$ state of $Eu^{2+}$.

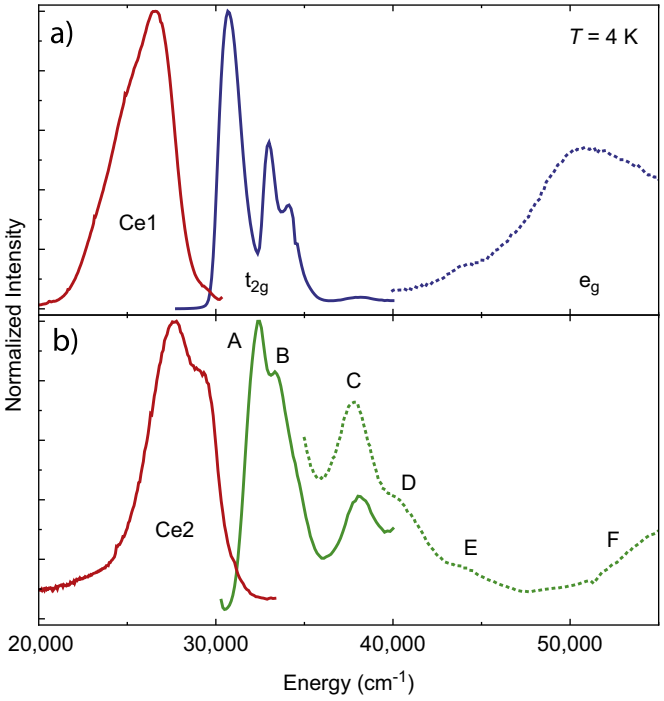


**Fig. 4.** Excitation and emission spectra of $Cs_2CaP_2O_7:Ce^{3+}$ (1%) at $T$ = 4 K. (a) Excitation (blue) and emission spectra (red) measured for $\lambda_{em} = 420$ nm and $\lambda_{exc} = 320$ nm. (b) Excitation (green) and emission spectra (red) measured for $\lambda_{em} = 340$ nm and $\lambda_{exc} = 262$ nm. The spectra recorded with the Edinburgh FLS 920 fluorescence spectrometer are the solid lines and the excitation spectra measured at the UVSOR facility are the dotted lines. (For interpretation of the references to color in this figure caption, the reader is referred to the web version of this paper.)

### 3.2. $Ce^{3+}$ luminescence

In this section we will present the luminescence properties of $Cs_2MP_2O_7:Ce^{3+}$. Usually the d–f emission properties of $Eu^{2+}$ and $Ce^{3+}$ are related [27]. Hence, we investigate if $Ce^{3+}$ also has an unusually large Stokes shift of emission in $Cs_2MP_2O_7$.

Figs. 4 and 5 show emission and excitation spectra at 4 K of $Cs_2CaP_2O_7:Ce^{3+}$ (1%) and $Cs_2SrP_2O_7:Ce^{3+}$ (1%), respectively. We have measured the luminescence of the samples for $\lambda_{exc} \sim 320$ nm (Figs. 4a and 5a) and $\lambda_{exc} \sim 260$ nm (Figs. 4b and 5b). For both excitation wavelengths the samples show a strong blue/UV emission, which is attributed to the parity-allowed $5d^1 \rightarrow 4f^1$ transition of $Ce^{3+}$. The blue luminescence is also visible with the naked eye (see Fig. S3). The lifetime of the emission is 28 ns, which is characteristic for the spin- and parity-allowed d–f transition of $Ce^{3+}$.

The emission spectra displayed in Figs. 4a and 5a ($\lambda_{exc} = 320$ nm (Ca) or 316 (Sr) nm) show the typical doublet emission band observed for $Ce^{3+}$ ions on a single lattice site (Ce1). The two emission bands are due to transitions from the lowest crystal field component of the $5d^1$ configuration to the $^2F_{5/2}$ and $^2F_{7/2}$ levels of the $4f^1$ ground state, which is split by spin-orbit coupling. The band of the lower-

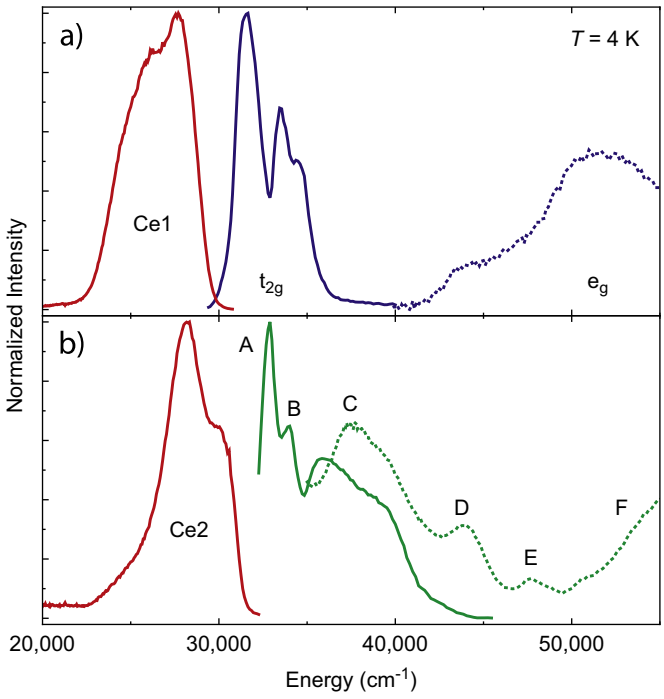


**Fig. 5.** Excitation and emission spectra of $Cs_2SrP_2O_7$:$Ce^{3+}$ (1%) at $T = 4$ K. (a) Excitation (blue) and emission spectra (red) measured with $\lambda_{em} = 410$ nm and $\lambda_{exc} = 316$ nm. (b) Excitation (green) and emission spectra (red) measured with $\lambda_{em} = 330$ nm and $\lambda_{exc} = 260$ nm. The spectra recorded with the Edinburgh FLS 920 fluorescence spectrometer are the solid lines and the excitation spectra measured at the UVSOR facility are the dotted lines. (For interpretation of the references to color in this figure caption, the reader is referred to the web version of this paper.)

energy $5d^1 \rightarrow {}^2F_{7/2}$ transition is weaker and therefore less apparent, especially for $Cs_2CaP_2O_7$:$Ce^{3+}$ were only a weak shoulder is observed around 25 000 $cm^{-1}$. The two peaks of the band are separated by $\sim$2000 $cm^{-1}$, which corresponds to the spin-orbit splitting of the $^2F$ ground state term of $Ce^{3+}$ [8].

Figs. 4b and 5b show that the shape of the $Ce^{3+}$ emission spectra is different when excitation is at $\sim$260 nm instead of $\sim$320 nm. This indicates that two different $Ce^{3+}$ emission sites are present in $Cs_2MP_2O_7$. The presence of two distinct $Ce^{3+}$ sites is confirmed by the excitation spectra shown in Figs. 4 and 5. The excitation spectra of the Ce1 and Ce2 emission both consist of several overlapping bands, which are attributed to $4f^1 \rightarrow 5d^1$ transitions of $Ce^{3+}$. However, it is observed that the structure, i.e. peak positions and splitting of the excitation spectra of the Ce1 emission band (see Figs. 4a and 5a) is significantly different from the excitation spectra recorded for the Ce2 emission (see Figs. 4b and 5b). This confirms that the local environment of the two $Ce^{3+}$ centers is different.

The splitting of the $5d^1$ state in the excitation spectra provides information on the local environment of the two $Ce^{3+}$ sites. $Ce^{3+}$ is in octahedral coordination in $Cs_2MP_2O_7$ and therefore a splitting of the $5d^1$ state into a $5d^1(t_{2g})$ and $5d^1(e_g)$ state is expected, the $t_{2g}$ state being lower in energy. For the lower energy Ce1 site (Fig. 4a and Fig. 5a), the excitation band between 30 000 and 40 000 $cm^{-1}$ is assigned to the $4f^1 \rightarrow 5d^1(t_{2g})$ transition. The $t_{2g}$ excitation band is split into three bands, which is explained by either a large spin–orbit coupling [19,28] or a slightly lower site symmetry for the $Ce^{3+}$ ion (distorted octahedron). The excitation band between 40 000 and 55 000 $cm^{-1}$ is assigned to the $4f^1 \rightarrow 5d^1(e_g)$ transition. In the excitation spectra of the higher energy Ce2 site (Fig. 4b and Fig. 5b) we identify six $4f^1 \rightarrow 5d^1$ excitation bands (A–F), which means that the $5d^1$ configuration is split into at least six different states. This indicates that the symmetry of the Ce2 site is much lower than (slightly distorted) octahedral.

The formation of two geometrically different $Ce^{3+}$ sites for $Cs_2MP_2O_7$:$Ce^{3+}$ is probably due to the charge compensation required for the $Ce^{\bullet}_{M^{2+}}$ site. The charge compensating defect can be local or distant, i.e. in the first shell of cations around the $Ce^{3+}$ ion or further away in the lattice. A distant defect will not influence the local geometry around the $Ce^{3+}$ ions, whereas a local defect can cause a deformation of the oxygen octahedron around the $Ce^{3+}$ ion. Hence, we expect that the (octahedral) Ce1 site is the distantly charge compensated site, whereas the lower symmetry Ce2 site has local charge compensation in $Cs_2MP_2O_7$. Alternatively, the extra $Ce^{3+}$ emission center can be in a second crystal phase doped with $Ce^{3+}$ ions. This however seems unlikely, as the XRD patterns in Fig. S1 show that no significant impurity crystal phases are present in our samples.

The crystal field splitting of the 5d configuration ($\epsilon_{cfs}$) for $Ce^{3+}$ in $Cs_2MP_2O_7$ can be estimated from the excitation spectra of the (slightly distorted) octahedral Ce1 site. The $\epsilon_{cfs}$ is calculated by taking the energy difference between the maxima of the $t_{2g}$ and $e_g$ excitation band. We find a $\epsilon_{cfs}$ of 20 346 and 19 736 $cm^{-1}$ for $Cs_2CaP_2O_7$ and $Cs_2SrP_2O_7$, respectively. The $\epsilon_{cfs}$ of the $Ce^{3+}$ 5d configuration is stronger in $Cs_2CaP_2O_7$, in agreement with the results for $Eu^{2+}$. There are several compounds for which the $\epsilon_{cfs}$ of the 5d configuration for both $Ce^{3+}$ and $Eu^{2+}$ is known. Using the data of these compounds, it was determined that the that $\epsilon_{cfs}$ in $Eu^{2+}$ is 0.77 times that in $Ce^{3+}$ [27]. If we compare the $\epsilon_{cfs}$ of $Eu^{2+}$ and $Ce^{3+}$ in $Cs_2MP_2O_7$, we find an $\epsilon_{cfs}(Eu^{2+})/\epsilon_{cfs}(Ce^{3+})$ ratio of 0.87 and 0.83 for $Cs_2CaP_2O_7$ and $Cs_2SrP_2O_7$, respectively ($\epsilon_{cfs}$ values determined by taking the energy difference between the maxima of the $t_{2g}$ and $e_g$ band). These values are close to the 0.77 ratio determined in Ref. [27].

From the excitation and emission spectra in Figs. 4 and 5 we can determine the Stokes shift of the $Ce^{3+}$ emission of $Cs_2MP_2O_7$:$Ce^{3+}$. If the Stokes shift of the $Ce^{3+}$ emission is anomalously large like the Stokes shift of the $Eu^{2+}$ d–f emission, this would indicate that also substantial electronic relaxation occurs in the 5d excited state of $Ce^{3+}$. The Stokes shift ($\Delta S$) of the $Ce^{3+}$ emission is defined as the difference between the energy $E^{abs}$ of the transition from the $4f^1\ {}^2F_{5/2}$ ground state to the lowest $5d^1$ excited state and the peak energy $E^{em}$ of the emission band belonging to the reverse $5d^1 \rightarrow {}^2F_{5/2}$ transition. $E^{abs}$ is the peak energy of the lowest-energy excitation band in the excitation spectra. The $E^{abs}$, $E^{em}$ and $\Delta S$ values determined for the Ce1 and Ce2 emission centers in $Cs_2CaP_2O_7$ and $Cs_2SrP_2O_7$ are listed in Table 2.

Before we discuss the $\Delta S$, let us consider the absorption energy $E^{abs}$ and emission energy $E^{em}$. For both emission centers, the energy $E^{abs}$ of the $Ce^{3+}$ $4f^1 \rightarrow 5d^1$ transition is lower for $Cs_2CaP_2O_7$ compared to $Cs_2SrP_2O_7$. This is attributed to the stronger crystal-field splitting for $Ce^{3+}$ in $Cs_2CaP_2O_7$. The $E^{em}$ is lower for $Cs_2CaP_2O_7$:$Ce^{3+}$ (both Ce1 and Ce2), which is in agreement with the results obtained for $Eu^{2+}$. The values for $E^{abs}$ and $E^{em}$ of $Cs_2MP_2O_7$:$Ce^{3+}$ are also in agreement with what is typically found for $Ce^{3+}$ in phosphate host lattices [29,30].

**Table 2**
Optical properties of $Ce^{3+}$ ions in $Cs_2CaP_2O_7$ and $Cs_2SrP_2O_7$. Estimated energy of the lowest $4f^1 \rightarrow 5d^1$ absorption band $E^{abs}$, peak energy of the $5d^1 \rightarrow {}^2F_{5/2}$ emission band $E^{em}$, and the Stokes shift $\Delta S = E^{abs} - E^{em}$. All values are in $cm^{-1}$ and at $T = 4$ K.

| Host | $E^{abs}$ | $E^{em}$ | $\Delta S$ |
|---|---|---|---|
| $Cs_2CaP_2O_7$:Ce1 | 30 675 | 26 738 | 3937 |
| $Cs_2SrP_2O_7$:Ce1 | 31 546 | 27 624 | 3922 |
| $Cs_2CaP_2O_7$:Ce2 | 32 468 | 29 499 | 2969 |
| $Cs_2SrP_2O_7$:Ce2 | 32 895 | 30 211 | 2684 |

In Table 2 it can be seen that for $Cs_2CaP_2O_7$:$Ce^{3+}$ the Stokes shift of the Ce1 emission center ($\Delta S = 3937\ cm^{-1}$) is larger than the Stokes shift of the Ce2 emission center ($\Delta S = 2969\ cm^{-1}$). A similar result is observed for $Cs_2SrP_2O_7$:$Ce^{3+}$. The Stokes shift values of both emission centers are in the range of $\Delta S = 1000$–$5000\ cm^{-1}$ that is typically observed for $Ce^{3+}$ in (phosphate) compounds [29,15]. This is in contrast with the Stokes shift obtained for the $Eu^{2+}$ d–f emission in $Cs_2MP_2O_7$, which is unusually large.

The $E^{abs}$ and $\Delta S$ values of $Ce^{3+}$ and $Eu^{2+}$ in $Cs_2MP_2O_7$ can be compared quantitatively using relations that have been determined by Dorenbos [27]. In Ref. [27] it was shown that the redshift of absorption, the Stokes shift of emission, the centroid shift of the 5d configuration and the total crystal field splitting of the 5d levels of $Eu^{2+}$ and $Ce^{3+}$ all appear to be linearly related to one another. The relations for $E^{abs}$ and $\Delta S$ are [27]:

$$E^{abs}(Eu^{2+}) = (0.64 \pm 0.02)E^{abs}\left(Ce^{3+}\right) + (0.53 \mp 0.06)\ eV, \quad (3)$$

$$\Delta S(Eu^{2+}) = (0.61 \pm 0.03)\Delta S(Ce^{3+}). \quad (4)$$

We use the results of $Cs_2MP_2O_7$:$Eu^{2+}$ and Eqs. (3) and (4) to predict the $E^{abs}$ and $\Delta S$ of $Ce^{3+}$ in $Cs_2CaP_2O_7$ and $Cs_2SrP_2O_7$. The calculated $Ce^{3+}$ (calc) values for $E^{abs}$ and $\Delta S$ are listed in Table 3, together with the experimental values of $Eu^{2+}$ and the Ce1 and Ce2 emission centers. The data in Table 3 show a good agreement between the experimental $E^{abs}$ values of the Ce1 emission and $E^{abs}$ values calculated for $Ce^{3+}$. However, the experimental $E^{abs}$ values of the Ce2 sites are just outside the range predicted for $E^{abs}$. This discrepancy can be due to a weaker crystal field splitting for the locally charge compensated Ce2 site.

In contrast to $E^{abs}$, we observe large differences between the calculated and experimental values for the $Ce^{3+}$ Stokes shift in Table 2. The Stokes shift predicted for the $Ce^{3+}$ emission is more than 1.2 eV, which is larger than Stokes shifts experimentally observed for $Eu^{2+}$ ($\sim 0.75$ eV). The Stokes shifts obtained for $Ce^{3+}$ from the spectra in Figs. 4 and 5 are however significantly smaller, with values of 0.3–0.5 eV for the Ce1 and Ce2 emission centers. It is clear that the Stokes shift of $Eu^{2+}$ and $Ce^{3+}$ in $Cs_2MP_2O_7$ do not show any relation. The observation of a normal Stokes shift for $Ce^{3+}$ indicates that only weak electronic relaxation takes place in the 5d excited state, and consequently there is no evidence for a substantial excited state deformation as suggested for $Eu^{2+}$ in $Cs_2MP_2O_7$.

### 3.3. Ytterbium luminescence

We have synthesized ytterbium doped $Cs_2CaP_2O_7$ and $Cs_2SrP_2O_7$ to investigate the d–f luminescence of $Yb^{2+}$ ions in $Cs_2MP_2O_7$. The d–f luminescence of $Yb^{2+}$ and $Eu^{2+}$ are expected to be related [31] and therefore the Stokes shift of the $Yb^{2+}$ emission may also be unusually large. In contrast to $Ce^{3+}$ions, $Yb^{2+}$ ions require no charge compensation when substituted into $Cs_2MP_2O_7$. As a consequence, $Yb^{2+}$-doped $Cs_2MP_2O_7$ will better resemble $Cs_2MP_2O_7$:$Eu^{2+}$.

The syntheses of Yb-doped $Cs_2CaP_2O_7$ and $Cs_2SrP_2O_7$ were carried out under a reducing atmosphere (10% $H_2$/90% $N_2$) to reduce the $Yb^{3+}$ ions of the Yb-precursor ($Yb_2O_3$) to $Yb^{2+}$ ions. However, no $Yb^{2+}$ d–f luminescence was observed for $Cs_2MP_2O_7$:Yb, even down to 4 K. Furthermore, no $Yb^{2+}$ f–d absorption band was visible in the diffuse reflection spectra between 300 and 400 nm. We instead did observe $Yb^{3+}$ $^2F_{5/2} \rightarrow {}^2F_{7/2}$ f–f luminescence for Yb-doped $Cs_2MP_2O_7$ (see Fig. S4). These observations indicate that Yb is not stable in the divalent state in $Cs_2MP_2O_7$. Indeed, of all the lanthanides, Eu is most easily reduced to the divalent state and also in the Eu-doped $Cs_2MP_2O_7$ luminescence of $Eu^{3+}$ ions was observed. Based on this, it is not surprising that $Yb^{2+}$ cannot be stabilized in $Cs_2MP_2O_7$. Since no $Yb^{2+}$ luminescence is measured, no comparison can be made between the luminescence properties of $Eu^{2+}$ and $Yb^{2+}$ ions in $Cs_2CaP_2O_7$ and $Cs_2SrP_2O_7$.

**Table 3**
4f→5d absorption energy $E^{abs}$ and Stokes shift $\Delta S$ of $Eu^{2+}$ and $Ce^{3+}$ in $Cs_2CaP_2O_7$ and $Cs_2SrP_2O_7$. The values displayed for $Ce^{3+}$ (calc) were determined using Eqs. (3) and (4). Ce1 and Ce2 represent the two different $Ce^{3+}$ emission centers observed for $Cs_2MP_2O_7$:$Ce^{3+}$. All values are in eV.

| Property | $Eu^{2+}$ | $Ce^{3+}$ (calc) | Ce1 | Ce2 |
|---|---|---|---|---|
| $E^{abs}$ (Ca) | 2.85 | $3.63 \pm 0.21$ | 3.80 | 4.03 |
| $\Delta S$ (Ca) | 0.78 | $1.28 \pm 0.06$ | 0.49 | 0.37 |
| $E^{abs}$ (Sr) | 2.97 | $3.81 \pm 0.21$ | 3.91 | 4.08 |
| $\Delta S$ (Sr) | 0.75 | $1.23 \pm 0.06$ | 0.49 | 0.33 |

## 4. Conclusions

Previous reports have shown that the d–f luminescence of $Eu^{2+}$ ions in $Cs_2MP_2O_7$ (M = $Ca^{2+}$, $Sr^{2+}$) is characterized by an unusually large Stokes shift $\Delta S > 6000\ cm^{-1}$. To gain insight in the origin of this large Stokes shift, we investigated the d–f luminescence of $Eu^{2+}$ ions in $Cs_2MP_2O_7$ at cryogenic temperatures (down to 4 K). Furthermore, we compared the $Eu^{2+}$ luminescence to the d–f luminescence of $Ce^{3+}$ and $Yb^{2+}$ ions in $Cs_2MP_2O_7$. At cryogenic temperatures, a large energy shift of around $3500\ cm^{-1}$ between the sharp onsets of the $Eu^{2+}$ emission and excitation bands was observed. This is surprising as the emission and excitation onsets of a specific electronic transition usually coincide. The onset shift indicates that there is a substantial electronic relaxation in the $4f^65d^1$ excited state, which can be due to a Jahn-Teller like deformation in the excited state. As a consequence of this deformation, the emission occurs from a lower energy excited $4f^65d^1$ state, resulting in a very large Stokes shift.

$Cs_2MP_2O_7$:$Ce^{3+}$ showed UV/blue $Ce^{3+}$ d–f luminescence from two different $Ce^{3+}$ sites. The formation of two distinct $Ce^{3+}$ sites can be understood from the need for charge compensation for $Ce^{3+}$ ions on the $M^{2+}$ site. Contrary to $Eu^{2+}$, the emission for $Ce^{3+}$ showed a normal Stokes shift of 2500–$4000\ cm^{-1}$ and therefore the emission bands are at much higher energies than would be predicted from the energy of the $Eu^{2+}$ emission and the Dorenbos relations. The normal $Ce^{3+}$ Stokes shift indicates that, in contrast to $Eu^{2+}$, no Jahn–Teller like deformation takes place in the 5d state of $Ce^{3+}$. Unfortunately no $Yb^{2+}$ d–f luminescence was observed for $Cs_2MP_2O_7$:Yb.

The results in this work indicate that the large Stokes shift for the $Eu^{2+}$ emission of $Cs_2MP_2O_7$:$Eu^{2+}$ can be explained by a Jahn–Teller like deformation in the excited state. To confirm that a substantial deformation in the excited state occurs, it is interesting to try measure the changes in the local geometry around the $Eu^{2+}$ ion in the excited state, i.e. differences in the $Eu^{2+}$-$O^{2-}$ distances. An excellent technique to measure the local geometry around an impurity ion is X-ray absorption spectroscopy, more particularly, Extended X-ray Absorption Fine Structure (EXAFS) and X-ray absorption Near Edge Structure (XANES) [32]. Recently, time-resolved x-ray absorption spectroscopy (TR-XAS) experiments have been used to measure local geometric changes in the excited state of various organometallic complexes and metal ions in solids [33–35]. Hence, future experiments with EXAFS and XANES are interesting for investigating the geometric structure in the $Eu^{2+}$ $4f^65d^1$ excited state.

## Acknowledgments

We thank Prof. M. Kitaura, Prof. J. Ueda and K. Asami, MSc for their help and skillful assistance in the VUV experiments at the UVSOR facility (UVSOR project number 27-515). The support of the UVSOR (Okazaki, Japan) is gratefully acknowledged. This work is financially supported by Technologiestichting STW, which is part of the Nederlandse Organisatie voor Wetenschappelijk Onderzoek (NWO).

## Appendix A. Supplementary data

Supplementary data associated with this paper can be found in the online version at http://dx.doi.org/10.1016/j.jlumin.2016.04.050.

## References

[1] P. Dorenbos, J. Lumin. 104 (4) (2003) 239.
[2] P. Dorenbos, J. Phys. Condens. Matter 15 (17) (2003) 2645.
[3] S.H.M. Poort, H.M. Reijnhoudt, H.O.T. van der Kuip, G. Blasse, J. Alloys Compd. 241 (1–2) (1996) 75.
[4] S.H.M. Poort, A. Meijerink, G. Blasse, J. Phys. Chem. Solids 58 (9) (1997) 1451.
[5] K. Van den Eeckhout, P.F. Smet, D. Poelman, Materials 3 (4) (2010) 2536.
[6] B.M.J. Smets, Mater. Chem. Phys. 16 (3–4) (1987) 283.
[7] C. Feldmann, T. Jüstel, C.R. Ronda, P.J. Schmidt, Adv. Funct. Mater. 13 (7) (2003) 511.
[8] G. Blasse, B.C. Grabmaier, Luminescent Materials, Springer-Verlag, Heidelberg, 1994.
[9] P.F. Smet, A.B. Parmentier, D. Poelman, J. Electrochem. Soc. 158 (6) (2011) R37.
[10] F. Suyver, A. Meijerink, Chemisch2Weekblad 98 (4) (2002) 12.
[11] A.M. Srivastava, H.A. Comanzo, S. Camardello, S.B. Chaney, M. Aycibin, U. Happek, J. Lumin. 129 (9) (2009) 919.
[12] A.M. Srivastava, H.A. Comanzo, S. Camardello, M. Aycibin, U. Happek, ECS Trans. 25 (9) (2009) 201.
[13] M. Marsman, J. Andriessen, C.W.E. van Eijk, Phys. Rev. B 61 (24) (2000) 16477.
[14] J. Andriessen, O.T. Antonyak, P. Dorenbos, P.A. Rodnyi, G.B. Stryganyuk, C.W. E. van Eijk, A.S. Voloshinovskii, Opt. Commun. 178 (4–6) (2000) 355.
[15] P. Dorenbos, J. Andriessen, M. Marsman, C.W.E. van Eijk, Radiat. Eff. Defects Solids 154 (3–4) (2001) 237.
[16] J. Andriessen, E. van der Kolk, P. Dorenbos, Phys. Rev. B 76 (7) (2007) 075124.
[17] S. Lizzo, A.H. Velders, A. Meijerink, G.J. Dirksen, G. Blasse, J. Lumin. 65 (6) (1995) 303.
[18] Z. Pan, L. Ning, B.-M. Cheng, P.A. Tanner, Chem. Phys. Lett. 428 (1–3) (2006) 78.
[19] L. van Pieterson, M.F. Reid, R.T. Wegh, S. Soverna, A. Meijerink, Phys. Rev. B 65 (4) (2002) 045113.
[20] V. Bachmann, C. Ronda, A. Meijerink, Chem. Mater. 21 (10) (2009) 2077.
[21] A. Meijerink, G. Blasse, J. Lumin. 43 (5) (1989) 283.
[22] S.H.M. Poort, W. Janssen, G. Blasse, J. Alloys Compd. 260 (1–2) (1997) 93.
[23] B. Henderson, G.F. Imbusch, Optical Spectroscopy of Inorganic Solids, Clarendon Press, Oxford, 1989.
[24] M. de Jong, L. Seijo, A. Meijerink, F.T. Rabouw, Phys. Chem. Chem. Phys. 17 (26) (2015) 16959.
[25] L.L. Chase, Phys. Rev. Lett. 23 (6) (1969) 275.
[26] L.L. Chase, Phys. Rev. B 2 (7) (1970) 2308.
[27] P. Dorenbos, J. Phys. Condens. Matter 15 (27) (2003) 4797.
[28] R.W. Schwartz, P.N. Schatz, Phys. Rev. B 8 (7) (1973) 3229.
[29] P. Dorenbos, J. Lumin. 91 (3–4) (2000) 155.
[30] P. Dorenbos, Phys. Rev. B 64 (12) (2001) 125117.
[31] P. Dorenbos, J. Phys. Condens. Matter 15 (3) (2003) 575.
[32] D.C. Koningsberger, R. Prins, X-Ray Absorption: Principles, Applications, Techniques of EXAFS, SEXAFS and XANES, Wiley-Interscience, Hoboken, 1987.
[33] E. Vorobeva, S.L. Johnson, P. Beaud, C.J. Milne, M. Benfatto, G. Ingold, Phys. Rev. B 80 (13) (2009) 134301.
[34] R.M. Van Der Veen, C.J. Milne, A.E. Nahhas, F.A. Lima, V.T. Pham, J. Best, J.A. Weinstein, C.N. Borca, R. Abela, C. Bressler, M. Chergui, Angew. Chemie – Int. Ed. 48 (15) (2009) 2711–2714.
[35] A. El Nahhas, R.M. van der Veen, T.J. Penfold, V.T. Pham, F.A. Lima, R. Abela, A. M. Blanco-Rodriguez, S. Záliš, A. Vlček, I. Tavernelli, U. Rothlisberger, C. J. Milne, M. Chergui, J. Phys. Chem. A 117 (2) (2013) 361–369.